

mechanisms, it is possible that the product of a specific ORF affects IRES function and, thus, influences the EGFP/DsRed readout in that particular cell. There will also be cases where the EGFP fusion may affect stability by affecting folding or obscuring degron sequences. Despite these limitations, this method offers a very deep window into a critical aspect of cellular physiology. The only other comprehensive global analysis of protein turnover that has been available was performed in budding yeast by using >3800 individual cycloheximide-chase analyses (28), a method that is impractical for mammalian cells.

A number of general findings emerged from this analysis. We found a bimodal distribution of protein half-lives centered around 0.5 and 2 hours. A similar distribution was previously observed in yeast, although with a shorter scale (28), which may be explained by the shorter cell cycle of yeast (~2 hours) compared with mammalian cells (~20 hours). We also find that longer proteins are relatively more stable. One possible explanation is that cells require more resources to synthesize longer proteins and tend to protect their investment. Although PEST sequences (polypeptide sequences enriched in proline, glutamic acid, serine, and threonine) are widely thought to be associated with short-half-life proteins (30), we found no enrichment of PEST sequences in labile proteins. Instead, unstable proteins appear to be rich in amino acids that can be phosphorylated, such as tyrosine and threonine. Indeed, phosphorylation is frequently a signal for regulated protein degradation (31). Thus, we conclude that the PEST hypothesis is incorrect in a general sense.

Proteins with unstructured regions (UPRs) are susceptible to degradation by the 20S proteasome *in vitro* (32). However, we found no correlation between the presence of UPRs (in both length and number) and protein instability. Because many UPRs function in molecular recognition, it is possible that *in vivo* UPRs are no longer “unstructured” and are protected by binding to their biological targets (33). Similar observations were made in yeast (34).

This GPS technology has a number of applications. It could be used to identify mutations that affect basal protein stability, which would reveal degron or stabilization sequences. GPS profiling could also be used to identify proteins whose stabilities change in response to stimuli, as well as during developmental transitions. GPS can be used to discover ubiquitin ligases or other proteins that regulate the stability of a protein of interest by coupling GPS with loss-of-function (from RNA interference) or gain-of-function screens that alter the DsRed/EGFP ratio. Conversely, this method could be used to identify substrates of ubiquitin ligases, currently a very labor-intensive endeavor with few general solutions, as we have done with the Skp1–cullin–F-box (SCF) ubiquitin ligase (35). GPS could be coupled with chemical screens to search for compounds that destabilize a protein of

interest as opposed to inhibiting its activity by direct binding. GPS profiling could also be used to generate disease-specific protein stability signatures that may be useful for both diagnosis and elucidation of disease mechanisms. Finally, the integration of global protein stability information with other data sets will provide a global vision of regulatory networks with greater clarity and will help identify cross-talk between protein turnover and other levels of biological regulation (36, 37). Thus, GPS has opened many avenues for protein-turnover studies.

References and Notes

1. S. Ghaemmaghami *et al.*, *Nature* **425**, 737 (2003).
2. S. F. Kingsmore, *Nat. Rev. Drug Discov.* **5**, 310 (2006).
3. J. M. Pratt *et al.*, *Mol. Cell. Proteomics* **1**, 579 (2002).
4. R. W. King, R. J. Deshaies, J. M. Peters, M. W. Kirschner, *Science* **274**, 1652 (1996).
5. V. Jesenberger, S. Jentsch, *Nat. Rev. Mol. Cell Biol.* **3**, 112 (2002).
6. A. Hershko, A. Ciechanover, *Annu. Rev. Biochem.* **67**, 425 (1998).
7. K. I. Nakayama, K. Nakayama, *Nat. Rev. Cancer* **6**, 369 (2006).
8. A. Ciechanover, A. L. Schwartz, *Biochim. Biophys. Acta* **1695**, 3 (2004).
9. A. L. Schwartz, A. Ciechanover, *Annu. Rev. Med.* **50**, 57 (1999).
10. L. Banks, D. Pim, M. Thomas, *Trends Biochem. Sci.* **28**, 452 (2003).
11. G. Nalepa, M. Rolfe, J. W. Harper, *Nat. Rev. Drug Discov.* **5**, 596 (2006).
12. Y. Sun, *Cancer Biol. Ther.* **2**, 623 (2003).
13. J. R. Newman *et al.*, *Nature* **441**, 840 (2006).
14. A. Sigal *et al.*, *Nature* **444**, 643 (2006).
15. A. Sigal *et al.*, *Nat. Methods* **3**, 525 (2006).
16. Materials and methods are available as supporting material on Science Online.
17. S. M. Ngoi, A. C. Chien, C. G. Lee, *Curr. Gene Ther.* **4**, 15 (2004).
18. T. V. Pestova *et al.*, *Proc. Natl. Acad. Sci. U.S.A.* **98**, 7029 (2001).
19. S. Matsuzawa, M. Cuddy, T. Fukushima, J. C. Reed, *Proc. Natl. Acad. Sci. U.S.A.* **102**, 14982 (2005).
20. Single-letter abbreviations for the amino acid residues are as follows: A, Ala; C, Cys; D, Asp; E, Glu; F, Phe; G, Gly; H, His; I, Ile; K, Lys; L, Leu; M, Met; N, Asn; P, Pro; Q, Gln; R, Arg; S, Ser; T, Thr; V, Val; W, Trp; and Y, Tyr.
21. M. Welcker *et al.*, *Mol. Cell* **12**, 381 (2003).
22. X. Ye *et al.*, *J. Biol. Chem.* **279**, 50110 (2004).
23. J. Jin *et al.*, *Genes Dev.* **17**, 3062 (2003).
24. D. M. Koepf *et al.*, *Science* **294**, 173 (2001).
25. M. Scheffner, J. M. Huibregtse, R. D. Vierstra, P. M. Howley, *Cell* **75**, 495 (1993).
26. D. Lane, E. Harlow, *Nature* **298**, 517 (1982).
27. J. F. Rual *et al.*, *Genome Res.* **14**, 2128 (2004).
28. A. Belle, A. Tanay, L. Bitincka, R. Shamir, E. K. O'Shea, *Proc. Natl. Acad. Sci. U.S.A.* **103**, 13004 (2006).
29. K. L. Rock *et al.*, *Cell* **78**, 761 (1994).
30. M. Rechsteiner, S. W. Rogers, *Trends Biochem. Sci.* **21**, 267 (1996).
31. T. Hunter, *Mol. Cell* **28**, 730 (2007).
32. S. Prakash, L. Tian, K. S. Ratliff, R. E. Lehotzky, A. Matouschek, *Nat. Struct. Mol. Biol.* **11**, 830 (2004).
33. G. Asher, N. Reuven, Y. Shaul, *Bioessays* **28**, 844 (2006).
34. P. Tompa, J. Prilusky, I. Silman, J. L. Sussman, *Proteins* **71**, 903 (2008).
35. H.-C. S. Yen, S. J. Elledge, *Science* **322**, 923 (2008).
36. T. Ideker *et al.*, *Science* **292**, 929 (2001).
37. T. J. Griffin *et al.*, *Mol. Cell. Proteomics* **1**, 323 (2002).
38. We thank M. Vidal, J.W. Harper, G. Hu, and J. Jin for the hORFome v1.1 library; J. Daly and S. Lazo-Kallanian for FACS assistance; and J. Love, S. Gupta, and K. Hurov for helpful discussions. H.-C.S.Y. is a Jane Coffin Childs Memorial Fund fellow. D.M.C. is supported by the National Science Foundation. This work is supported by an NIH grant AG11085 to J.W.H. and S.J.E. S.J.E. is an investigator with the Howard Hughes Medical Institute.

Supporting Online Material

www.sciencemag.org/cgi/content/full/322/5903/918/DC1
Materials and Methods
Figs. S1 to S5
Tables S1 to S6
14 May 2008; accepted 22 September 2008
10.1126/science.1160489

Identification of SCF Ubiquitin Ligase Substrates by Global Protein Stability Profiling

Hsueh-Chi Sherry Yen and Stephen J. Elledge*

Ubiquitin-mediated proteolysis regulates all aspects of cellular function, and defects in this process are associated with human diseases. The limited number of identified ubiquitin ligase–substrate pairs is a major bottleneck in the ubiquitin field. We established and applied genetic technologies that combine global protein stability (GPS) profiling and genetic perturbation of E3 activity to screen for substrates of the Skp1–cullin–F-box (SCF) ubiquitin ligase in mammalian cells. Among the >350 potential substrates identified, we found most known SCF targets and many previously unknown substrates involved in cell cycle, apoptosis, and signaling pathways. Exploring cell cycle–stage stability, we found that several substrates used the SCF and other E3s in different cell cycle stages. Our results demonstrate the potential of these technologies as general platforms for the global discovery of E3–substrate regulatory networks.

The selective degradation of proteins is an important means of regulating gene expression and has pivotal roles in the control of various cellular processes. Ubiquitin (Ub)–mediated proteolysis is the major nonlysosomal proteolytic

pathway in the cell and is required for the degradation of key regulatory proteins that include tumor suppressors, oncoproteins, and cell cycle regulators. Most proteins degraded by this pathway are first tagged with polyubiquitin chains by

the sequential action of three classes of enzymes: E1 (Ub-activating enzyme), E2 (Ub-conjugating enzyme), and E3 (Ub ligase). Once ubiquitinated, proteins are rapidly hydrolyzed by the 26S proteasome. Substrate specificity is largely conferred by E3 Ub ligases, and the interaction of substrates with E3s is the major point of regulation in Ub-mediated protein turnover (1).

There are more than 500 E3s in the human genome, but functional information is available for only a small fraction. Linking an E3 with its substrates is difficult and is generally dependent on either a functional connection or a physical association between the proteins. Given the large number of ubiquitinated substrates and E3s, more efficient strategies to deduce E3-substrate pairs are needed. Performing biochemical screens for E3 substrates is labor-intensive and is hampered by low substrate levels and intrinsically weak interactions between E3s and their substrates. Many E3s participate in human disease (2, 3). Thus, elucidating E3-substrate interactions is not only critical to further our understanding of normal protein turnover control and its deregulation in disease, but may also provide valuable information for the development of new therapeutic intervention strategies.

The SCF ubiquitin ligase is a modular RING-type E3 and consists of at least four components: Skp1, Cul1, Rbx1, and an F-box protein. Cul1 functions as a scaffold that simultaneously interacts with Rbx1, coupled to an E2 enzyme, and with Skp1 to recruit an F-box protein, the subunit responsible for substrate recognition (4–6). About 70 F-box proteins have been discovered in humans, and several have been shown to be involved in diseases, such as Skp2 and Fbw7 in cancer (7, 8). Many SCF substrates have been identified and are involved in a broad range of cellular functions that include cell cycle progression (e.g., cyclins and Cdc25A); signal transduction (e.g., Notch and inhibitor of nuclear factor κ B); and transcription (e.g., SMAD and c-Jun) (7, 9).

Here, we present the development of high-throughput approaches to provide a general solution for E3 substrate identification. We used global protein stability (GPS) profiling (10), coupled with genetic ablation of E3 function, to isolate new SCF substrates (11). We demonstrated the feasibility of these approaches through confirmation of known substrates and the discovery of a large number of new substrates. In addition to their use in E3 target identification, these strategies can be further generalized to detect proteins whose stabilities increase or decrease in response to various drugs or stimuli.

Inhibition of SCF activity by dominant-negative Cul1. To search for substrates of the SCF in vivo, we developed methods to quickly ablate cellular

Cul1 function. Prolonged SCF inhibition has the potential to alter cell cycle distribution and to confound our analysis. Because Cul1 is very stable, we applied a dominant-negative (DNCul1), instead of small interfering RNA, to reduce Cul1 activity. To monitor SCF activity, we established reporter human embryonic kidney HEK 293T

cell lines expressing enhanced green fluorescent protein (EGFP) fused to Cdc25A or p21^{CIP1}, two known SCF substrates, from the GPS reporter cassette (10). In these cells, *Discosoma* sp. red fluorescent protein (DsRed) and EGFP-fusions are expressed under the control of the same promoter, and thus the EGFP/DsRed ratio reflects

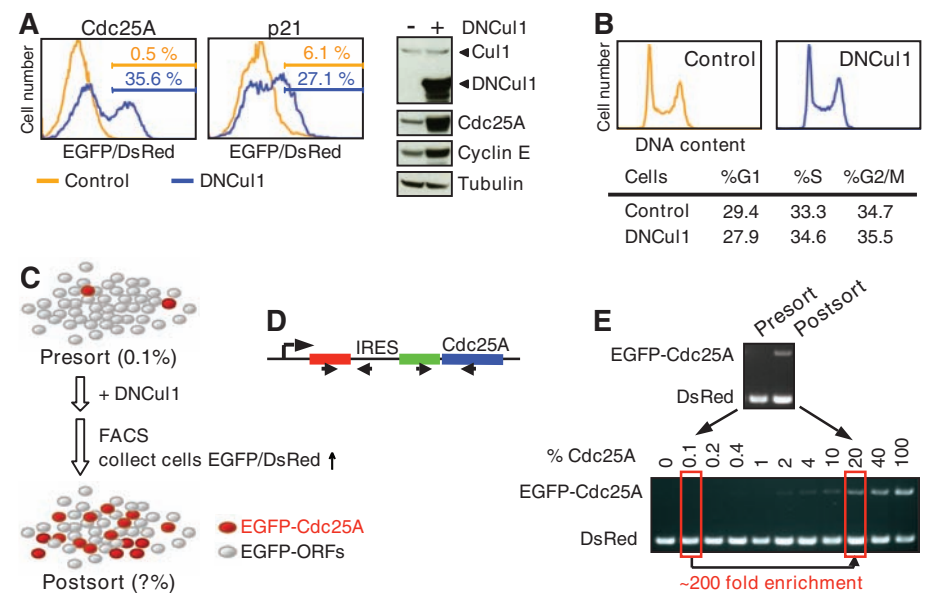


Fig. 1. A proof-of-principle screen for SCF substrates. (A) HEK 293T cells expressing DsRed-IRES-EGFP-Cdc25A or DsRed-IRES-EGFP-p21 were infected with either control or DNCul1 viruses for 18 hours and the EGFP/DsRed ratios of cells were measured by FACS. The abundance of Cul1 and endogenous SCF targets was analyzed by Western blot. (B) The cell cycle profile of HEK 293T cells infected with control or DNCul1 viruses for 18 hours was analyzed by propidium iodide staining. (C) Schematic illustration of the proof-of-principle screen. (D) Arrows represent PCR primers for DsRed and EGFP-Cdc25A. (E) Genomic DNA from presorted, postsorted, and various EGFP-Cdc25A and library cell mixtures was subjected to PCR and analyzed by agarose gel electrophoresis.

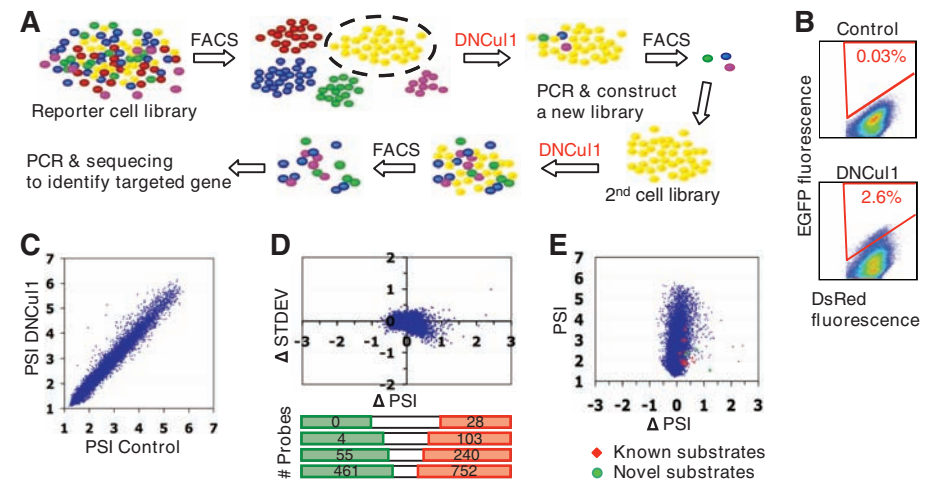


Fig. 2. Isolation of SCF targets by GPS profiling. (A) Schematic for the enrichment approach to E3 substrate identification. Cells with different EGFP/DsRed ratios are labeled with different colors. Shown here are the procedures for two rounds of enrichment. (B) The EGFP and DsRed fluorescence of a secondary cell library infected with control or DNCul1 viruses. (C) The PSI of EGFP-ORFs in control or DNCul1 virus-infected cells. (D) Changes in PSI and SD (STDEV) (Δ = DNCul1 minus control) were plotted, and the number of probes matching various ranges of Δ PSI is shown on the bottom of the graph. Note that some ORFs have two probes spotted on each microarray. (E) A plot of the PSI versus Δ PSI. Results from probes against previously discovered SCF targets are colored red, and those from probes against ICAT, APBB1IP, and FBXL14 are marked in green.

Department of Genetics, Center for Genetics and Genomics, Brigham and Women's Hospital, Howard Hughes Medical Institute, Harvard Medical School, Boston, MA 02115, USA.

*To whom correspondence should be addressed. E-mail: selledge@genetics.med.harvard.edu

the stability of the EGFP-fusion protein and is not affected by changes in transcription (10). Blocking SCF activity should result in accumulation of EGFP-Cdc25A and EGFP-p21 and should increase EGFP/DsRed ratios. We compared several delivery conditions and found that lentiviral delivery of DNCul1 provided the most potent inhibition. As soon as 18 hours after viral infection, ~30% of reporter cells displayed an increased EGFP/DsRed ratio, and endogenous SCF substrates accumulated as well (Fig. 1A). Note that because the degradation of Cdc25A and p21 depends on cell cycle stage-specific phosphorylation, not all cells shift their EGFP/DsRed ratio in asynchronous cultures. The amount of DNCul1 sufficient for substrate stabilization under this condition did not alter the cell cycle profile of these cells, which made it possible to search for SCF targets without the confounding effects of cell cycle perturbation (Fig. 1B).

A proof-of-principle screen. We constructed a HEK 293T reporter cell library expressing EGFP fused to ~8000 human open reading frames (ORFs) from the GPS reporter cassette in their genome (10). Because the EGFP/DsRed ratio of these cells reflects the stability of the EGFP-fusion protein, SCF targets can be detected in cells that show increased EGFP/DsRed ratios in response to Cul1 inhibition. To test our ability to identify SCF substrates, we added cells carrying EGFP-Cdc25A into the EGFP-ORF cell library to see whether those EGFP-Cdc25A cells were recovered with our screen (Fig. 1C). EGFP-Cdc25A-expressing cells were mixed with EGFP-ORF library cells at a ratio of 1 to 1000 and infected with DNCul1 viruses. Cells with elevated EGFP/DsRed ratios were collected by fluorescence-activated cell sorting (FACS). To distinguish Cdc25A from library cells, genomic DNA was isolated and subjected

to polymerase chain reaction (PCR) with two pairs of primers, one for DsRed and the other for EGFP-Cdc25A (Fig. 1D). The percentage of EGFP-Cdc25A cells in a mixed population was estimated by the ratio of PCR-amplified EGFP-Cdc25A to DsRed (Fig. 1E, bottom). The proportion of EGFP-Cdc25A cells in the FACS-isolated population increased to ~20%, a 200-fold enrichment compared with the starting mixture (Fig. 1E). These results support the idea that an enrichment strategy can identify SCF substrates.

Screening for SCF substrates by GPS profiling.

We used two methods for identifying SCF substrates using GPS profiling with conditional Cul1 inactivation. The first method entailed presorting the reporter cell library into sublibraries with narrow, but defined, ranges of EGFP/DsRed ratios by FACS. Within each individual subpopulation, cells that showed increased EGFP/DsRed ratios in response to Cul1 inhibition were collected, and ORFs were recovered by PCR. Isolated ORFs were either sequenced or used to construct a secondary cell library for further enrichment (Fig. 2A). We applied two-rounds of selection with one sublibrary and identified enriched clones as predicted by our Cdc25A enrichment test (Fig. 2B and fig. S1). By sequencing 48 randomly chosen clones, we obtained 11 unique genes and confirmed that four of these encode proteins degraded by SCF, including p21^{CIP1} and three novel substrates, ICAT (inhibitor of β -catenin and Tcf-4), APBB1IP (β -amyloid precursor protein-binding, family B, member 1-interacting protein), and FBXL14 (F-box and leucine-rich-repeat protein 14) (Figs. 3 and 4). The recovery of both known and new targets indicates that enrichment is a feasible method for substrate identification.

The second and more powerful approach used GPS profiling coupled with microarray deconvolution (10). In brief, the library cells infected with control or DNCul1 lentiviruses were fractionated into seven pools on the basis of their EGFP/DsRed ratios. The ORF sequences acting as unique identifiers for reporter cells were isolated from the genomic DNA from each pool by PCR amplification and quantified by microarray hybridization (fig. S2). The protein stability index (PSI) and standard deviation (SD), representing stability deviation from the mean, of each EGFP-ORF was calculated from the hybridization signals (10). SCF targets were identified by comparing the PSI of ORFs expressed in cells with and without DNCul1 virus infection.

We performed a series of analyses and confirmed that the quality of our microarray hybridization is high (11) (table S1). We plotted the PSI of each EGFP-ORF protein from control and DNCul1-expressing cells and observed a high correlation coefficient of 0.982 with a slope of nearly 1 (1.079) (Fig. 2C). The high degree of identity between PSIs from cells with and without DNCul1 supports the reliability of the array approach for measuring protein stability and confirms that most EGFP-ORF proteins are not tar-

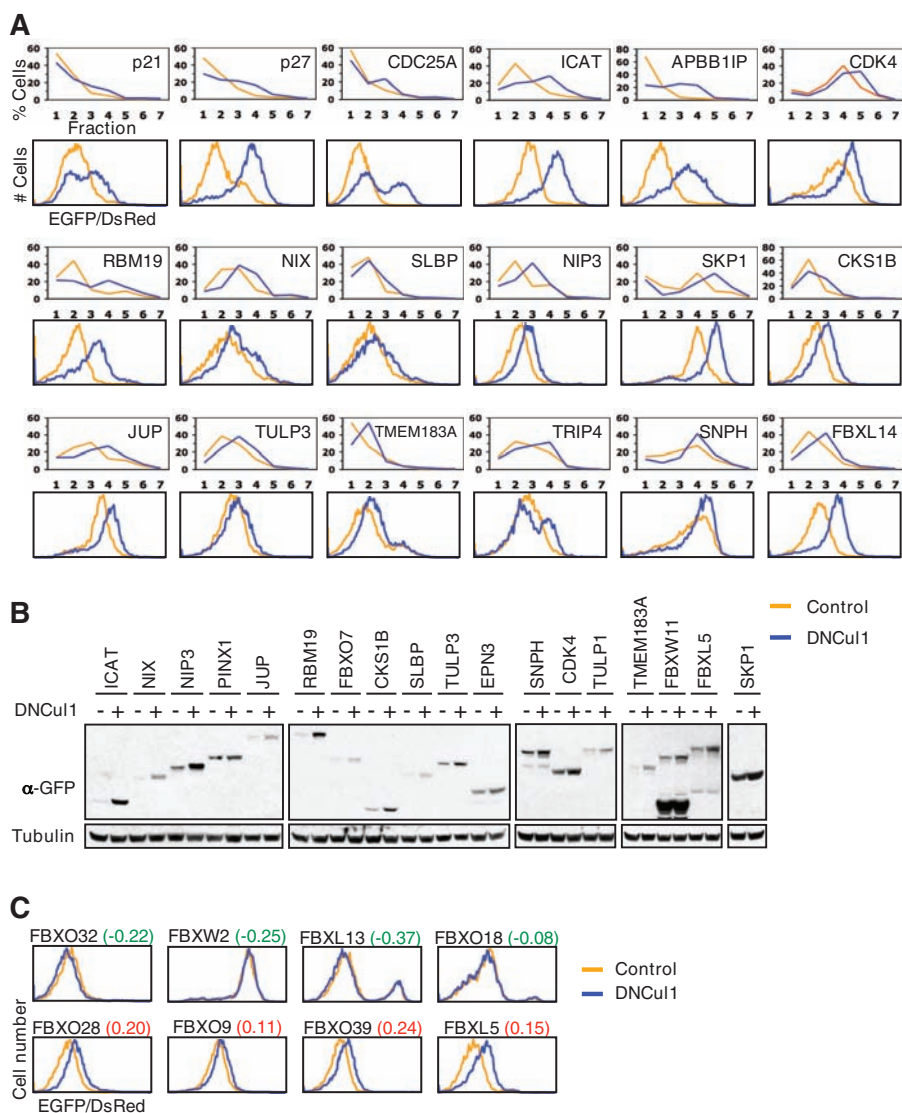


Fig. 3. Screen validation. **(A)** Comparison between the EGFP/DsRed profiles derived from the microarray data (top) and from individual FACS analyses (bottom). **(B)** The EGFP-ORF protein level in cells expressing the indicated GFP fusion protein infected with control (-) or DNCul1 (+) viruses. **(C)** The EGFP/DsRed ratios of cells infected with control or DNCul1 viruses were analyzed by FACS. The number shown at the top of each graph is the Δ PSI of the indicated F-box protein from the screen.

ged by the SCF. We calculated the difference in PSI with and without DNCu1 ($\Delta = \text{DNCu1 minus control}$) and found more ORFs with increased stability than decreased stability after SCF inhibition (Fig. 2D). Because inhibiting the SCF should lead to stabilization, the detection of more ORFs with a positive ΔPSI supports the validity of this approach. Because noise from low hybridization signals can be a problem for microarray-based detection, we examined the relation between ΔPSI and hybridization signal. Low signals were not the reason for the observed stability variation (fig. S3).

To further assess the validity of this strategy, we examined the behavior of known SCF substrates in the screen. We detected a significant ΔPSI for 73% (11 of 15) of previously described SCF substrates present in the library (Fig. 2E and table S2). Moreover, all three novel substrates isolated from our enrichment screen, ICAT, APBB1IP, and FBXL14, were also recovered. These analyses collectively reveal that our experimental approach is capable of global isolation of E3 substrates.

SCF substrate validation. We selected ORFs for subsequent validation studies by the following criteria. First, to reduce false-positives generated from spurious hybridization, we stipulated that the Cy5 channel signal for a given probe had to be greater than fivefold above background, and the variation in Cy5 intensity of the same probe between chips must be less than threefold. Second, the PSI had to increase more than 0.25 units when SCF was inhibited. The selection of this threshold was referenced to the ΔPSI of known SCF substrates. Third, we focused on proteins that are normally unstable, that is, the PSI of those proteins from control cells must be less than 3.3. Last, for ORFs with two probes, results from both probes had to be consistent. As a result, 359 ORFs met these criteria, and we chose 66 ORFs independent of their known functions for validation (table S3).

As an initial validation of the hits from our screen, ORFs encoding potential SCF substrates were individually recombined into the GPS reporter to create stable cell lines. Each reporter cell line was infected with either control or DNCu1 viruses, and their EGFP/DsRed ratios were measured by FACS. Clones with increased EGFP/DsRed in response to DNCu1 expression were independently tested at least three times. Of the 66 tested, we confirmed 31 lines whose EGFP/DsRed ratio was dependent on the SCF (Table 1). We next compared the EGFP/DsRed profile derived from the microarray data with those from individual FACS analysis. The EGFP/DsRed pattern from bulk analysis with the microarray was similar to that from single-tube FACS (Fig. 3A), which suggested that the isolation of those ORFs was not due to spurious factors. The advantage of this microarray-based method is that it identifies targets and also precisely reports the stability of a protein and its degree of change after SCF inhibition. We further confirmed protein abundance by Western blot analysis of cell extracts with antibodies to EGFP (Fig. 3B). The validation rate sug-

gests that the signal-to-noise ratio of this screen is high and demonstrates the robustness of this approach as a general method to identify E3 substrates.

Validated proteins include 6 previously reported and 25 SCF substrates not previously described that function in various cellular activities, including cell cycle progression, apoptosis, and signaling (Table 1). We also identified Skp1 and five F-box proteins that constitute the SCF itself. Because many E3 ligases control their own turnover, the isolation of SCF subunits suggests that their degradation might be mediated through autoubiquitination within the complex. In fact, two budding yeast F-box proteins, Cdc4p and Grr1p, have been shown to ubiquitinate themselves (12, 13). We therefore wondered whether the dependence on the SCF for turnover is a general feature for F-box proteins. After surveying our microarray data for every F-box protein in the library, we found that not all F-box proteins were stabilized after SCF inactivation (table S4). To explore this further, we randomly selected four F-box proteins that did not increase PSI after DNCu1 treatment and four that mildly increased but did not meet the criteria for validation ($\Delta\text{PSI} > 0.25$) and tested them by FACS. The results were consistent with those from the screen (Fig. 3C). Thus, degradation by the SCF is not a universal feature of all F-box proteins. The recovery of a large number of previously described substrates together with the high validation rate supports the idea that many proteins on the candidate substrate list are likely to be bona fide targets of the SCF.

To further examine the validity of this method, we tested whether the observed degradation by SCF depends on the N-terminal EGFP fusion. We analyzed the amount of either endogenous proteins (Fig. 4A) or proteins tagged with a single

copy of hemagglutinin (HA) at the C terminus (Fig. 4B) in cells with and without DNCu1. In most cases (89%, 17 of 19), proteins accumulated to greater steady-state amounts after loss of SCF activity (Table 1). Because ORF-HA proteins were expressed under the control of the ubiquitously active elongation factor EF1 α promoter whose activity is not affected by the SCF, the detected increase in protein abundance is likely due to an increase in protein stability and not synthesis. To confirm it, we measured the half-life of proteins in cells in which protein synthesis had been inhibited with cycloheximide. All tested proteins were stabilized in cells infected with DNCu1 viruses (Fig. 4C), which suggested that the EGFP/DsRed ratio serves as a reliable indicator of protein stability. To test whether the SCF substrates isolated from HEK 293T cells are also targeted by the SCF in other cell types, we analyzed the amounts of endogenous proteins for which antibodies are available (Fig. 4D). The proteins accumulated in response to DNCu1 in most cell types, but the degree of accumulation was cell-type specific, which suggested that various cell types may have distinct combinations of proteolysis pathways (for example, differential expression profiles of F-box proteins).

SCF substrates and the cell cycle. A unique feature of GPS is its ability to monitor protein turnover at the resolution of single living cells. Measuring the average of a cell population can overlook events that happen in only a subset of cells, all-or-none effects, and variability between cells. We combined GPS and Hoechst staining for DNA content to study cell cycle-mediated protein degradation by three-color FACS analysis. We expressed several cell cycle proteins from the GPS cassette and found that cells that carry

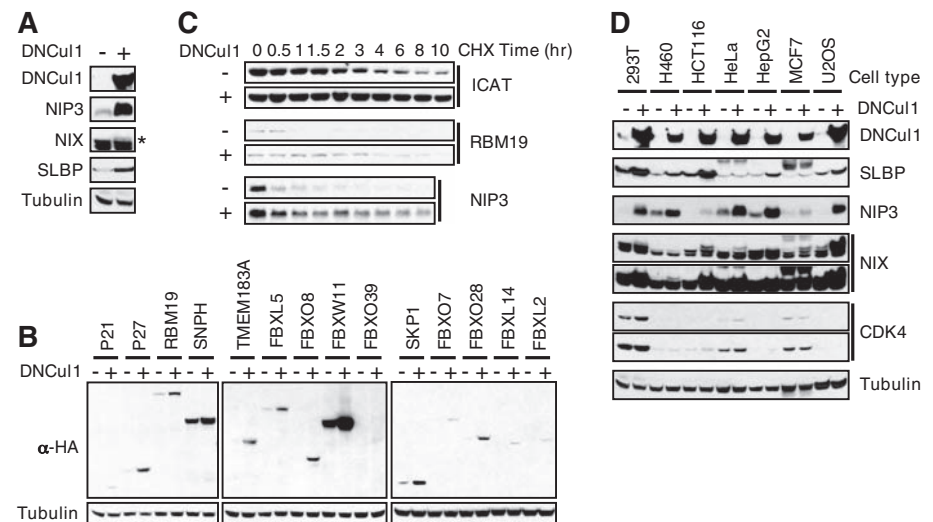


Fig. 4. SCF substrate validation. (A) The amount of endogenous proteins in HEK 293T cells infected with either control (–) or DNCu1 (+) viruses analyzed by Western blot. Asterisk (*) indicates the protein band representing NIX according to its molecular weight. (B) Western blot analysis of the indicated HA-tagged ORFs from cells infected with either control (–) or DNCu1 (+) viruses. HA-ORFs were expressed under the control of the EF1 α promoter and introduced into HEK 293T cells by retroviral infection at low MOI. (C) Protein stability measured by cycloheximide (CHX)-chase. (D) The level of endogenous proteins in various cell lines infected with control (–) or DNCu1 (+) viruses. Results from two exposure times are shown for NIX and CDK4.

EGFP-Cdc20, -cyclin A, -cyclin E, and -securin fusion proteins displayed more divergent EGFP/DsRed ratios than those of the control EGFP-degron cell series (10) (Fig. 5A). We found that cells expressing EGFP-Cdc20, but not the control, d4EGFP (mutant of a degron with $t_{1/2}$ of 4 hours), show distinct EGFP/DsRed ratios in cells with different DNA contents (Fig. 5B), which indicates that the variability in EGFP/DsRed ratios is due to differences in stabilities in different cell cycle stages. Consistent with the fact that Cdc20 is degraded by the anaphase-promoting complex/cyclosome APC/C^{CDH1} during late mitosis (14, 15), two populations of EGFP/DsRed ratios were observed from EGFP-Cdc20-expressing cells with G₂/M DNA content, with the lowest observed EGFP/DsRed ratio in G₁ cells. Thus, GPS combined with Hoechst staining provides a way to rapidly identify proteins whose turnovers are cell cycle-regulated.

Many proteins with cell cycle-regulated stabilities are controlled by the SCF, so we wondered if some SCF substrates identified from our

screen might also be cell cycle-regulated. Indeed, the half-lives of p27, stem-loop binding protein (SLBP), and syntaphilin (SNPH) varied during cell cycle progression (Fig. 5C and fig. S4A). The stabilization of p27 in G₁ and SLBP during S phase is consistent with previous reports (16, 17), and their known cell cycle stage-specific functions. We found SNPH, a protein involved in mitochondrial docking and vesicular transport (18), is unstable specifically in G₁. We next asked whether the degradation of these proteins by the SCF is restricted to a particular cell cycle stage (Fig. 5D and fig. S4B). For some proteins, the stabilization by DNCu1 was more pronounced in, but not restricted to, specific cell cycle stages, such as p27 and tubby like protein 3 (TULP3) during S and G₂ phases and Bcl2/adenovirus E1B 19-kD-interacting protein 3 (NIP3) and Cdc28 protein kinase regulatory subunit 1B (CKS1B) during S phase (Fig. 5D). In contrast, degradation of SLBP and SNPH by the SCF is specifically limited to G₂/M and G₁ phase cells, respectively. Although SLBP was unstable in both the G₁ and

G₂/M phases (Fig. 5C), stabilization of SLBP by DNCu1 was detected only at G₂/M (Fig. 5D), which suggested that there are at least two distinct ligases or pathways regulating SLBP turnover: the SCF in G₂/M and an unknown ligase in G₁.

The phosphorylation of threonines 61 and 62 is required for SLBP degradation but the E3 ligase remains unidentified (16). We mutated the two threonines to alanines and found that the mutations led to G₂/M phase-specific stabilization of SLBP (Fig. 5E). Furthermore, the half-life of mutant SLBP was no longer regulated by the SCF. The EGFP/DsRed profile of cells expressing mutated SLBP with or without DNCu1 is the same as that of cells carrying wild-type SLBP with DNCu1 at all cell cycle stages, which suggests that threonines 61 and 62 are essential components of the degron responsible for SCF-mediated degradation.

The assignment of substrates to their cognate E3 enzymes has proven difficult and has primarily relied on physical association (19–21) or the presence of known degron motifs (22, 23), or has depended on genetic screens in model organisms (24–28). Each of these methods has significant drawbacks and, so far, has identified only a few dozen substrates in total. A recent study in yeast suggested that in vivo screens may serve as a better alternative for identifying physiologically relevant E3 substrates (29). They isolated SCF^{Grr1} substrates by using the budding yeast ORF-GFP fusion strain collections mated to *grr1* mutants and sporulated in a 96-well format followed by quantitative microscopy. As the GFP fusions used were under control of their endogenous promoters, the results were confounded to some degree by transcriptional control. Although the method was successful, it is, unfortunately, not applicable to mammals.

In this study, we employed GPS profiling coupled with either an enrichment strategy or a microarray deconvolution approach to search for SCF substrates in mammalian cells. Using a library of ~8000 ORFs, we successfully isolated both previously reported and novel SCF substrates, which demonstrated the potential of these technologies as systematic platforms for high-throughput discovery of E3 substrates. Our results from the microarray-based screen are particularly encouraging. We recovered 73% of previously described SCF substrates in our library and generated a list of likely substrates containing 359 proteins. Individual FACS measurements confirmed 31 of the 66 tested proteins as bona fide substrates. Furthermore, results from ORFs with only a slight increase in stability were readily reproducible. The low false-positive and false-negative rates of the screen are favorable compared with those of most high-throughput microarray-based approaches. Approximately 300 candidate substrates from the screen remain to be characterized, and we conservatively estimate that as many as 100 SCF substrates or more may be identified by this screen. This is an underestimate of the total number of SCF substrates because the current library is not

Table 1. Summary of validation results. The asterisk (*) marks the ORF-HA proteins whose expression was not detected by Western blot. Because ORF-HA was expressed as a single copy from the genome, it is likely that a single HA epitope tag is insufficient for the detection of low-abundance proteins. Proteins that were not tested are labeled N/A (not assessed). Except APBB1IP, all ORFs isolated from the screen are full-length. ID, identification.

Protein name	Gene ID	Δ PSI	Known?	FACS	Western blot	
					Anti-GFP	Anti-HA or endogenous
APBB1IP/PREL1	54518	1.22	No	+	+	N/A*
ICAT/CTNBP1	56998	0.72	No	+	+	N/A*
RBM19	9904	0.67	No	+	+	+
NIX/BNIP3L	665	0.46	No	+	+	+
SLBP	7884	0.28	No	+	+	+
ARMCX6	54470	0.33	No	+	N/A	N/A*
PINX1	54984	0.55	No	+	+	–
EPN3	55040	0.57	No	+	+	–
TMEM183A	92703	0.26	No	+	+	+
NIP3/BNIP3	664	0.33	No	+	+	+
CKS1B	1163	0.31	No	+	+	N/A*
CDK2AP1	8099	0.32	No	+	N/A	N/A*
AASDHPPT	60496	0.27	No	+	N/A	+
FBXL14	144699	0.43	No	+	+	+
FBXL2	25827	0.43	No	+	N/A	+
TRIP4	9325	0.36	No	+	N/A	+
SKP1	6500	0.72	No	+	+	+
FBXO7	25793	0.26	No	+	+	+
SNPH	9751	0.42	No	+	+	+
PYROXD1	79912	0.27	No	+	N/A	+
FBXW11	23291	0.32	No	+	+	+
CDK4	1019	0.45	No	+	+	+
JUP	3728	0.41	No	+	+	N/A
TULP1	7287	0.36	No	+	+	N/A
TULP3	7289	0.45	No	+	+	N/A
p21	1026	0.37	Yes	+	+	+
p27	1027	0.64	Yes	+	+	+
CDC25A	993	0.29	Yes	+	+	+
NFKBIB	4793	0.32	Yes	+	N/A	N/A
USP18	11274	0.28	Yes	+	N/A	N/A
FBXO5	26271	0.27	Yes	+	N/A	N/A

complete, and the detection of some substrates may require an extended disruption of SCF activity. Moreover, the screen was performed in only a single cell type, which may not fully express the F-box proteins for some substrates or the signaling pathway components, such as kinases, needed to target proteins for degradation. These circumstances probably explain why some of the known SCF substrates thought to be present in the library were not identified in the screen. In addition, we cannot rule out the possibility that the EGFP fusion affects SCF-mediated degradation in a protein-specific manner.

We performed an analysis on the distribution of GO processes associated with the 359 candidate substrates and found that these proteins are involved in diverse cellular functions with a minor enrichment in apoptosis, which suggests that the SCF plays critical roles in a broad range of cellular activities and is not limited to cell cycle regu-

lation. For example, ICAT is a negative regulator of the Wnt pathway. ICAT inhibits β -catenin nuclear signaling by binding to β -catenin and competing for its interaction with TCF transcription factors (30). The *ICAT* gene is located at a frequent target for LOH in many human cancers (31). Conversely, the F-box protein required for its degradation may act as an oncogene. NIX and NIP3 are functional homologs and members of the BCL2/adenovirus E1B-interacting protein family (32, 33). NIX and NIP3 are transcriptionally induced during hypoxia, and their expression promotes apoptosis (34). Both NIX and NIP3 are degraded by the proteasome (33). SNPH regulates synaptic vesicle docking and fusion by inhibiting the SNARE (soluble *N*-ethylmaleimide-sensitive factor attachment protein receptor) complex and is required for proper distribution of mitochondria within axons on neurons (18, 35). SNPH was unstable in G₁, and its degradation by the SCF is

G₁-specific. The pivotal role of the SCF in cell cycle progression was further highlighted through our identification of cell cycle proteins as novel SCF substrates, such as CKS1B, a Cdk-binding protein that is also an accessory protein necessary for SCF^{Skp2} to target p27 degradation (36), and SLBP, the sole cell cycle-regulated factor required for histone mRNA processing (16, 37). Overexpression of CKS1B has been observed in many tumors and correlates with poor prognosis (38). The stability of SLBP is regulated during the cell cycle, but the E3s controlling its degradation are not known (16). We found that there are distinct pathways mediating SLBP turnover at G₁ and G₂/M, and the degradation of SLBP by SCF is G₂/M-specific and requires the phosphorylation of threonines 61 and 62. We also found several substrates, such as CKS1B, NIP3 and TULP3, that did not show cell cycle-regulated stability but, nonetheless, showed cell cycle-stage differences in their SCF-dependent degradation. This suggests the existence of other E3s that work together with the SCF to control their degradation throughout the cell cycle.

Although inactivation of an E3 was our variable parameter, it is clear that the described system could be used to identify proteins whose stabilities change because of a number of different stimuli or genetic perturbations. Thus, one could envision looking for proteins whose stabilities change in response to chemical or physical stimuli such as DNA damage or hormones. Various screens could be performed with specific protein fusions from this expression cassette to identify pathways or chemicals that control its stability. The use of GPS profiling to measure perturbation of protein stability adds a new dimension to our ability to examine the proteome and provides a step toward the goal of a systems-level understanding of cellular physiology.

References and Notes

1. A. L. Schwartz, A. Ciechanover, *Annu. Rev. Med.* **50**, 57 (1999).
2. G. Nalepa, J. Wade Harper, *Cancer Treat. Rev.* **29** (suppl. 1), 49 (2003).
3. L. T. Vassilev *et al.*, *Science* **303**, 844 (2004).
4. N. Zheng *et al.*, *Nature* **416**, 703 (2002).
5. C. Bai *et al.*, *Cell* **86**, 263 (1996).
6. D. Skowrya, K. L. Craig, M. Tyers, S. J. Elledge, J. W. Harper, *Cell* **91**, 209 (1997).
7. T. Cardozo, M. Pagano, *Nat. Rev. Mol. Cell Biol.* **5**, 739 (2004).
8. J. T. Winston, D. M. Koepf, C. Zhu, S. J. Elledge, J. W. Harper, *Curr. Biol.* **9**, 1180 (1999).
9. K. I. Nakayama, K. Nakayama, *Nat. Rev. Cancer* **6**, 369 (2006).
10. H.-C. S. Yen, Q. Xu, D. M. Chou, Z. Zhao, S. J. Elledge, *Science* **322**, 918 (2008).
11. Materials and methods are available as supporting material on Science Online.
12. P. Zhou, P. M. Howley, *Mol. Cell* **2**, 571 (1998).
13. J. M. Galan, M. Peter, *Proc. Natl. Acad. Sci. U.S.A.* **96**, 9124 (1999).
14. G. Fang, H. Yu, M. W. Kirschner, *Mol. Cell* **2**, 163 (1998).
15. S. Prinz, E. S. Hwang, R. Visintin, A. Amon, *Curr. Biol.* **8**, 750 (1998).
16. L. Zheng *et al.*, *Mol. Cell Biol.* **23**, 1590 (2003).
17. A. C. Carrano, E. Eytan, A. Hershko, M. Pagano, *Nat. Cell Biol.* **1**, 193 (1999).
18. J. S. Kang *et al.*, *Cell* **132**, 137 (2008).
19. J. Jin, X. L. Ang, T. Shirogane, J. Wade Harper, *Methods Enzymol.* **399**, 287 (2005).

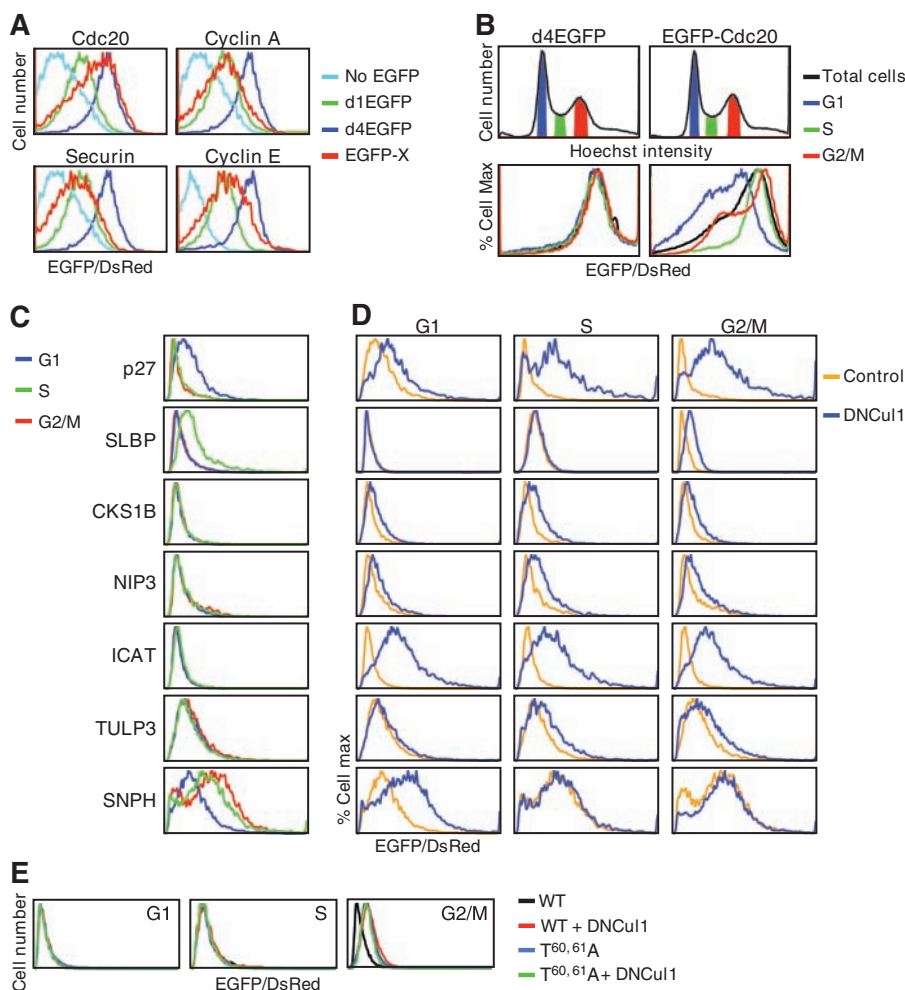


Fig. 5. SCF substrate stability and the cell cycle. **(A)** Overlay of the EGFP/DsRed ratios of EGFP-degron fusions (d1EGFP, $t_{1/2}$ = 1 hour; d4EGFP, $t_{1/2}$ = 4 hours) and EGFP fused to cell cycle proteins, as indicated in the graph. **(B)** Asynchronous cells expressing EGFP-Cdc20 fusions or the d4EGFP control from the GPS cassette were colored with Hoechst stain and analyzed by FACS. The EGFP/DsRed profiles of the asynchronous population or cells at a specific cell cycle stage, as judged by the DNA content, were compared. **(C)** Cells expressing EGFP-fused SCF substrates were analyzed as **(B)**. **(D)** The EGFP/DsRed ratio of cells with control or DNCu1 viruses at different cell cycle stages. **(E)** The EGFP/DsRed ratio of cells carrying either wild-type or Thr^{61,62}Ala-mutated SLBP infected with control or DNCu1 viruses.

20. D. M. Koepf *et al.*, *Science* **294**, 173 (2001).
 21. F. Margottin *et al.*, *Mol. Cell* **1**, 565 (1998).
 22. C. M. Pfeleger, M. W. Kirschner, *Genes Dev.* **14**, 655 (2000).
 23. J. T. Winston *et al.*, *Genes Dev.* **13**, 270 (1999).
 24. S. M. Slepka *et al.*, *Cell* **129**, 1011 (2007).
 25. K. H. Moberg, D. W. Bell, D. C. Wahrer, D. A. Haber, I. K. Hariharan, *Nature* **413**, 311 (2001).
 26. E. Spencer, J. Jiang, Z. J. Chen, *Genes Dev.* **13**, 284 (1999).
 27. J. Jiang, G. Struhl, *Nature* **391**, 493 (1998).
 28. D. C. Nelson, J. Lasswell, L. E. Rogg, M. A. Cohen, B. Bartel, *Cell* **101**, 331 (2000).
 29. J. A. Benanti, S. K. Cheung, M. C. Brady, D. P. Toczyski, *Nat. Cell Biol.* **9**, 1184 (2007).
 30. K. Tago *et al.*, *Genes Dev.* **14**, 1741 (2000).
 31. J. Reifenberger *et al.*, *Int. J. Cancer* **100**, 549 (2002).
 32. J. M. Boyd *et al.*, *Cell* **79**, 341 (1994).
 33. G. Chen *et al.*, *J. Biol. Chem.* **274**, 7 (1999).
 34. R. K. Bruick, *Proc. Natl. Acad. Sci. U.S.A.* **97**, 9082 (2000).
 35. G. Lao *et al.*, *Neuron* **25**, 191 (2000).
 36. D. Ganoth *et al.*, *Nat. Cell Biol.* **3**, 321 (2001).
 37. Z. F. Wang, M. L. Whitfield, T. C. Ingledue 3rd, Z. Dominski, W. F. Marzluff, *Genes Dev.* **10**, 3028 (1996).
 38. S. Kitajima *et al.*, *Am. J. Pathol.* **165**, 2147 (2004).
 39. We thank M. Vidal, J. W. Harper, J. Jin, and G. Hu for the hORFeome v1.1 library; J. W. Harper for the DNCu1/pcDNA3 construct; D. M. Chou for experimental assistance and discussion; Q. Xu for bioinformatics analysis; M. Schlachach for microarray assistance; J. Daly

and S. Lazo-Kallanian for their help with cytometry; and K. Hurov for suggestions. H.-C.S.Y. is a fellow of Jane Coffin Childs Memorial Fund. This work was funded by an NIH grant AG 11085 to J. W. Harper and S.J.E. S.J.E. is an investigator with the Howard Hughes Medical Institute.

Supporting Online Material

www.sciencemag.org/cgi/content/full/322/5903/923/DC1
 Materials and Methods
 Figs. S1 to S4
 Tables S1 to S4

14 May 2008; accepted 22 September 2008
 10.1126/science.1160462

REPORTS

Slow Electron Cooling in Colloidal Quantum Dots

Anshu Pandey and Philippe Guyot-Sionnest*

Hot electrons in semiconductors lose their energy very quickly (within picoseconds) to lattice vibrations. Slowing this energy loss could prove useful for more efficient photovoltaic or infrared devices. With their well-separated electronic states, quantum dots should display slow relaxation, but other mechanisms have made it difficult to observe. We report slow intraband relaxation (>1 nanosecond) in colloidal quantum dots. The small cadmium selenide (CdSe) dots, with an intraband energy separation of ~ 0.25 electron volts, are capped by an epitaxial zinc selenide (ZnSe) shell. The shell is terminated by a CdSe passivating layer to remove electron traps and is covered by ligands of low infrared absorbance (alkane thiols) at the intraband energy. We found that relaxation is markedly slowed with increasing ZnSe shell thickness.

When semiconductors are formed into quantum dots (QDs), discrete electronic states arise through confinement by the boundary. These states can be exploited in optical applications, where size-tunable narrow fluorescence emissions with lifetimes in the nanosecond range are useful (1). However, such narrow fluorescence emission entails the dissipation of any initially absorbed excess energy as heat within hundreds of femtoseconds (2, 3). This rapid energy loss ("electron cooling") is not useful in electronics applications such as photovoltaics or infrared (IR) devices. Slower dissipation might give time to extract the energy of hot carriers for more efficient photovoltaics (4), and it would also enable the detection and emission of IR radiation via the intraband transitions of quantum dots.

In small QDs, such as colloidal CdSe, with a low electron mass, slow dissipation is in fact predicted on the basis that the lattice vibrations (30 meV) cannot couple widely separated electronic states (300 meV) (5–8) (Fig. 1B). The striking absence of such a "phonon bottleneck" in photoexcited QDs has been explained by fast excitonic cooling, where the electron transfers its

energy to the much larger density of states of the more massive hole (9–11) (Fig. 1C). Nonetheless, efforts to decouple the electron and hole led to marginally longer picosecond relaxation times (12–14), raising the possibility of other mechanisms involving local intermediate states, generically called traps (15, 16), and high-frequency local modes (17) or molecular vibrations (14).

In our experiments, electron cooling between the two lowest conduction band states of small colloidal CdSe dots, $1S_e$ and $1P_e$, is slowed to longer than 1 ns, which is more than three orders

of magnitude slower than the relaxation time between the $1S$ and $1P$ exciton (2). This slower cooling is achieved by using a thick ZnSe shell to separate electrons and holes and to increase the distance of the electronic states from the ligands. We observed three complementary mechanisms shown schematically in Fig. 1. With an exposed ZnSe surface, electron trapping takes place on a time scale of 10 to 30 ps (Fig. 1D). Capping the ZnSe shell with one monolayer (1 ML) of CdS reduces electron trapping, but it can also prevent hole trapping and allows fast excitonic cooling (<6 ps) (Fig. 1C). A CdSe capping monolayer reduces electron trapping as well, but with hole-trapping ligands, electron cooling slows from 10 ps to >1 ns, in agreement with a mechanism of energy transfer to vibrations via dipole coupling (Fig. 1E).

In our experiments, the electron in the conduction band state of the dots is photogenerated, which leaves a hole initially in the valence band. Reducing electron-hole coupling requires a shell that preserves electron confinement and extracts the hole to a remote state, as shown in Fig. 2A. To avoid intermediate local electronic states or vibrational modes that could arise at defects, the shell must be epitaxial, and its surface should have no states that would trap the electron. To limit coupling to ligand vibrations, the shell should be thick and its outer surface capped by ligands of low IR absorbance.

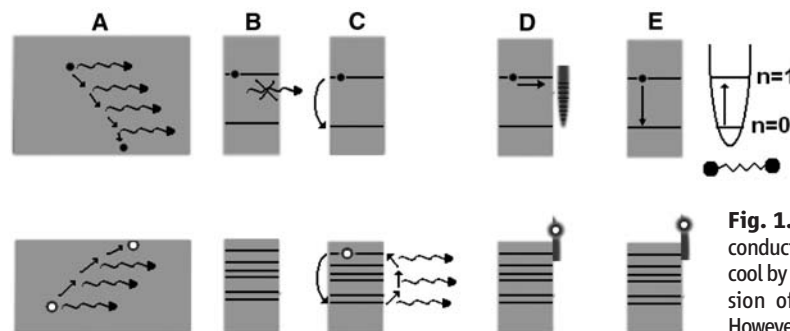


Fig. 1. (A) In bulk semiconductors, hot carriers cool by sequential emission of phonons. (B) However, in a small dot, electronic states are too

far apart for phonon emission. (C) An electron can cool by transferring its energy to the hole with higher state density that then relaxes via phonons. (D) With a reduced coupling to the hole, shown here as surface-trapped, the electron can cool via intermediate trap states. (E) The electron can transfer its energy to a resonant high-frequency vibration.

James Franck Institute, University of Chicago, 929 East 57th Street, Chicago, IL 60637, USA.

*To whom correspondence should be addressed. E-mail: pgs@uchicago.edu